Journal of the Mechanics and Physics of Solids 83 (2015) 88–103

Contents lists available at ScienceDirect

Journal of the Mechanics and Physics of Solids

journal homepage: www.elsevier.com/locate/jmps

Adhesion of heterogeneous thin films II: Adhesive heterogeneity

S.M. Xia [a], L. Ponson [b], G. Ravichandran [c], K. Bhattacharya [c,*]

[a] George W. Woodruff School of Mechanical Engineering, Georgia Institute of Technology, Atlanta, GA 30332, USA
[b] Institut Jean le Rond d'Alembert (UMR 7190), Sorbonne Universités, CNRS - UPMC, F-75005 Paris, France
[c] Division of Engineering and Applied Science, California Institute of Technology, Pasadena, CA 91125, USA

ARTICLE INFO

Article history:
Received 3 September 2014
Received in revised form
17 April 2015
Accepted 13 June 2015
Available online 20 June 2015

Keywords:
Adhesion
Heterogeneity
Directionality
Thin films
Fracture

ABSTRACT

This paper continues the study of the effective adhesion of thin films on rigid substrates in the presence of spatial heterogeneities started in Xia et al. (2013). In this paper, we focus on thin adhesive tape with spatial heterogeneity in the adhesive strength. This heterogeneity leads to a wavy peel front and consequently a complex corrugated shape in the tape. We develop a theory for the evolution of the peel front that accounts for this complex interaction, and an experimental method that is able to examine this in detail. We show through theory and experimentation that spatial patterning of the adhesive strength can lead to a very rich range of behaviors in the effective adhesive strength. In particular we show that adhesive heterogeneity can be used to create asymmetry in that the force required to peel the tape in one direction can be different from that in the other.

1. Introduction

This paper is the second part of our work on the effective adhesion of a heterogeneous thin film. In Part I of this work, we focused on the effects of elastic heterogeneity and demonstrated remarkable enhancement of effective adhesive strength through a combined theoretical and experimental study (Xia et al., 2013). In the present paper, we consider a different scenario where the elastic properties of the thin film are uniform but the intrinsic adhesion energy of the adhesive interface is heterogeneous.

Materials are inherently heterogeneous over a wide range of length scales: nano, micro and macro. Metallic alloys are heterogeneous at the nanoscale due to the various atomic constituents including interstitials and defects. Metallic and ceramic materials are heterogeneous at the microscale due to their polycrystalline nature and the presence of inclusions and precipitates. Composite materials are classical examples of heterogeneity arising from different phases and reinforcements in the form of particles and fibers. Heterogeneity is often linked to toughening of materials because of the ability of the reinforcing phase to impede and/or deflect crack growth. While considerable progress has been made towards understanding the effective elastic and inelastic properties (constitutive laws) of heterogeneous solids (e.g., Milton, 2002; Nemat-Nasser and Hori, 1999; Ponte Castañeda and Suquet, 1998, and references there), relatively little is known regarding their effective toughness. A number of analytical and computational studies have contributed to our understanding of the role of various heterogeneities on toughness of materials in specific examples (e.g., Bower and Ortiz, 1991, 1993; Hutchinson and

* Corresponding author. Fax: +1 626 583 4963.
E-mail address: bhatta@caltech.edu (K. Bhattacharya).

http://dx.doi.org/10.1016/j.jmps.2015.06.010
0022-5096/

Suo, 1992; Xu et al., 1998; Cox and Yang, 2006; Chen et al., 2008; Patinet et al., 2013b; Démery et al., 2014; Hossain et al., 2014, and references there). Kesari et al. (2010) and Kesari and Lew (2011) recently investigated the enhancement of effective macroscopic adhesion of rough surface contact with the use of adhesion instability. This work was later extended by Jin and Guo (2013) to understand the adhesion behavior of contact systems with both surface roughness and inhomogeneous material properties. Hutchinson and Suo (1992) have provided a comprehensive review of the mechanics and mechanisms of toughening of bi-materials and composites.

The present study develops insights concerning the role of heterogeneities on the overall toughness of materials using a model system of peeling a thin film (tape) from a periodically patterned heterogeneous adhesive substrate. While recent studies have focused on the role of random heterogeneity on effective toughness of materials, there has been no systematic study exploring the effects of periodic heterogeneity on effective fracture toughness. The underlying mathematical problem is that of a propagating front (discontinuity), which is impeded by obstacles. Such front propagation problems are important in many areas of materials science including phase boundaries (Dirr and Yip, 2006; Dondl and Bhattacharya, 2010; Craciun and Bhattacharya, 2004), dislocations (Hirth and Lothe, 1992; Patinet et al., 2011) and crack propagation (Rice, 1985; Legrand et al., 2011; Ponson and Bonamy, 2010). In the present study, we explore further the problem of a propagating wavy front in the context of peeling through a combined theoretical and experimental investigation.

The problem of peeling a homogeneous tape from a rigid substrate with uniform adhesive energy can be traced back to the seminal work of Rivlin (1944). This problem provides a simple one-dimensional framework for exploring fracture or front propagation problems. The problem of peeling is often modeled using either a one-dimensional membrane or Bernoulli–Euler beam theory. It was shown in Part-I of this work, that significant enhancement in peeling force can be attained through elastic heterogeneity of the film (Xia et al., 2013). By patterning the substrate with varying adhesive energies, the peel front is perturbed, i.e., no longer straight. The deviation of the peel front from being straight introduces additional bending in the direction normal to the direction of peeling. By appropriate choice of the adhesive patterning of the substrate, one can also introduce anisotropy and asymmetry in peeling that is reflected in the effective toughness of the system. These interesting and novel characteristics offered by adhesive heterogeneity could be potentially exploited in biomedical and engineering applications. Some early results of our study on adhesive heterogeneity were reported in Xia et al. (2012).

Problems in similar settings have been previously investigated mainly through experimentation. Ghatak et al. (2004) studied the peeling of a flexible plate from a patterned elastomeric substrate and found enhancement in peel force when compared to peeling from a uniform adhesive substrate. Chung and Chaudhury (2005) made similar observations who attributed the significant toughening to the sequential crack nucleation at heterogeneities at the interface. Ramrus and Berg (2006) conducted a series of experiments to characterize the adhesion of randomly patterned heterogeneous interfaces. Compared to homogeneous control specimens, adhesion enhancement due to heterogeneous micro-patterning was observed and attributed to arrest and confinement effects of crack propagation. Chan et al. (2007) used template-assisted silane treatment to obtain adhesive interfaces with more regular, periodically arranged patterns. Peel tests on these patterned interfaces showed that adhesion tuning was related to a characteristic length scale defined by the ratio of critical energy release rate and elastic modulus. More recently, Dalmas et al. (2009) and Patinet et al. (2013a) studied the crack arresting by tough pinning sites in a planar heterogeneous interface. They used a simple patterning technique to create a fracture toughness contrast in a weak interface of a double cantilever beam (DCB) sample. The effective adhesion properties of such heterogeneous interface, however, were not investigated in their work. Motivated by the biological structures such as gecko's feet, there has been considerable effort in achieving enhanced adhesion strength through 3D structures such as pillars and other features on the substrate (Greiner et al., 2007).

An exploration of adhesion directionality during peeling has been conducted in our study. It has been recognized that one can introduce adhesion anisotropy in the sense that crack fronts propagating along different axes can have different adhesion strengths. For example, the pull force along the spooling axis of a tape can be made different from the pull force across the tape (i.e., perpendicular to the spooling axis). Furthermore, the adhesion strength can be made to depend not only on the axis of the pull, but also on the direction with respect to the sense of the pull. This directionality of adhesion has been demonstrated by using an array of tilted microfibrils (Santos et al., 2007) to develop gecko-like adhesives for vertical climbing. Similar architectures were also used by others to achieve directional adhesion to water, for applications in interfacial propulsion (Prakash and Bush, 2011) and directional water shedding-off (Guo et al., 2012). In this study, we will show that it is not necessary to use such complex 3D microstructures to achieve directional adhesion; adhesive heterogeneity in a planar interface, if introduced at a right length scale, can give rise to the same adhesion behavior.

In Section 2, we describe a theoretical model for peeling of a thin film from a patterned adhesive substrate, which is based on the Kirchhoff plate theory via a variational formulation. The model provides predictions for the non-local energy release rate and its dependence on the peel-front perturbation. Section 3 describes the fabrication of a model material system and an experimental setup used for peel testing. The results of the experiments on various patterned substrates and comparison with theoretical predictions are presented in Section 4. The results for anisotropy and asymmetry in effective adhesion are also presented. Finally, the conclusions, implications and limitations of the present study, and directions for future study are summarized in Section 5.

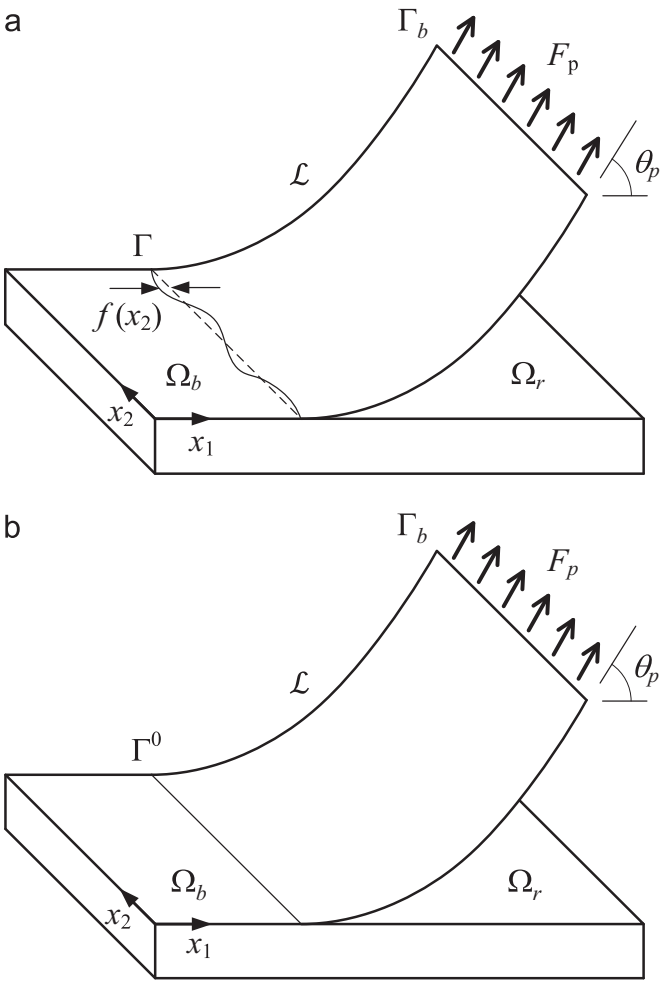

Fig. 1. Peeling of elastic thin films with (a) heterogeneous and (b) homogeneous distributions of intrinsic adhesion energy.

2. Theory

2.1. Framework

Consider a film being peeled from a substrate by the application of a force per unit width $F = F_p\{\cos\theta_p, 0, \sin\theta_p\}$ at one end, as shown in Fig. 1(a). We assume that the peel angle θ_p is held constant as the film is being peeled. We denote by $\Omega \in \mathbb{R}^2$ the flat reference configuration of the film, which is the union of Ω_r (the released portion) and Ω_b (the bonded portion). We also define the peeling front Γ and the extremity Γ_b of the film where the peeling force is applied (see Fig. 1(a)). Since the film is being peeled at a finite angle, the released portion undergoes very large deformation, and we cannot directly use small deformation plate theory. So we start with the finite deformation plate theory going back to Kirchhoff (1850). Specifically, we assume that the released portion of the film undergoes an isometric deformation y: $\Omega \to \mathbb{R}^3$: Material points of the film initially located in $x = \{x_1, x_2, 0\}$ before deformation are located in $y = \{y_1, y_2, y_3\}$ after deformation. The potential energy of the system is given by

$$\mathcal{E} = \int_{\Omega_r} \frac{D}{2}(\kappa_{11}^2 + \kappa_{22}^2 + 2\nu\kappa_{11}\kappa_{22} + (1-\nu)\kappa_{12}^2)\, dA - \int_{\Gamma_b} F\cdot y\, dl - \int_{\Omega_b} \gamma\, dA \tag{1}$$

where $\kappa = (\kappa_{ij})_{1\le i,j\le 2}$ is the curvature defined by $(\nabla y)^T\nabla n$. Here ∇ denotes the gradient with respect to x and thus ∇y: $\Omega \to \mathbb{R}^{3\times 2}$ or $\nabla y = (\partial y_i/\partial x_j)_{1\le i\le 3, 1\le j\le 2}$. $D = Eh^3/(12(1-\nu^2))$ is the bending stiffness of the film that depends on the film thickness h, its Young's modulus E and Poisson's ration ν. γ is the excess surface energy density of the released region compared to the bonded region. The first integral of Eq. (1) is the energy associated with bending the film while the second term is the potential energy of the applied (dead) force.

2.2. Scaling

We are interested in a situation where the adhesive interface is heterogeneous on a length-scale that is small compared to the width and length of the film, but large with respect to the film thickness h so that the plate theory applies. If the adhesive interface were homogeneous, we would expect the peel front to be straight as shown in Fig. 1(b). We can find the shape of the film exactly by using a Euler–Bernoulli beam theory (with the modulus adapted for a plate), and these details are presented in Xia et al. (2013). In the following, we will focus on heterogeneities introduced at small scales. So that we expect the peel front to be a small but rapidly varying perturbation from a straight line, and the deformed shape of the released portion of the film to be a small but rapidly varying perturbation of the singly bent surface. Therefore we linearize our equations about this known solution by making a Kirchhoff–Love hypothesis.

To this end, we assume that our peel front Γ as well as the deformation has a multi-scale form

$$y(x,\xi) = y^0(x) + \varepsilon u(x,\xi) \tag{2}$$

$$\Gamma = \{x\colon x = x^0 - \sqrt{\varepsilon} f(x_2/\sqrt{\varepsilon})\hat{e}_1\} \tag{3}$$

where $\xi = x/\sqrt{\varepsilon}$ is the fast variable. Notice that we have assumed that the amplitude of the deviation of the film from the singly curved interface is much smaller at $O(\varepsilon)$ compared to the variation in the heterogeneities, the front and the wavelength of the deviation all of which are at $O(\sqrt{\varepsilon})$. This is because the mechanics of the film is governed by bending (instead of stretching), and thus we seek finite perturbations in the curvature.

Introducing the unit normal $n = y_{,1}\times y_{,2}$ and the unit tangent $t_\alpha = y_{,\alpha} = (\nabla y)e_\alpha$ to the film in the α-direction, one obtains

$$t_\alpha = y_{,\alpha} = y^0_{,\alpha} + \varepsilon\left(u_{,\alpha} + \frac{1}{\sqrt{\varepsilon}}u_{,\tilde{\alpha}}\right) \approx y^0_{,\alpha} + \sqrt{\varepsilon}u_{,\tilde{\alpha}} \tag{4}$$

where the subscript '$,\alpha$' describes differentiation with respect to x_α while the subscript '$,\tilde{\alpha}$' describes differentiation with respect to the fast variable ξ_α. In approximating (4), only the leading term of order $O(\sqrt{\varepsilon})$ is kept. Similarly, up to the order of $O(\sqrt{\varepsilon})$, we have

$$\begin{aligned} n &= y_{,1}\times y_{,2}\\ &\approx (y^0_{,1} + \sqrt{\varepsilon}u_{,\bar{1}})\times(y^0_{,2} + \sqrt{\varepsilon}u_{,\tilde{2}})\\ &\approx y^0_{,1}\times y^0_{,1} + \sqrt{\varepsilon}(y^0_{,1}\times u_{,\tilde{2}} + u_{,\bar{1}}\times y^0_{,2}) + O(\varepsilon)\\ &\approx n^0 + \sqrt{\varepsilon}(y^0_{,1}\times u_{,\tilde{2}} + u_{,\bar{1}}\times y^0_{,2}). \end{aligned} \tag{5}$$

It then follows that

$$n_{,\beta} \approx n^0_{,\beta} + (y^0_{,1}\times u_{,\tilde{2}\tilde{\beta}} + u_{,\bar{1}\tilde{\beta}}\times y^0_{,2}), \tag{6}$$

and

$$\kappa_{\alpha\beta} = (\nabla y^T\nabla n)_{\alpha\beta} = y_{,\alpha}n_{,\beta} \approx \kappa^0_{,\alpha\beta} + y^0_{,\alpha}\cdot(y^0_{,1}\times u_{,\tilde{2}\tilde{\beta}} + u_{,\bar{1}\tilde{\beta}}\times y^0_{,2}), \tag{7}$$

where we only attain the leading terms of order $O(1)$.

Finally assume that the small perturbation u is always normal to the unperturbed film:

$$u(x, x/\sqrt{\varepsilon}) = w(x/\sqrt{\varepsilon})n^0(x) \quad \text{so that } u_{,\tilde{\alpha}} = w_{,\tilde{\alpha}}n^0. \tag{8}$$

Then, $\kappa_{\alpha\beta} \approx \kappa^0_{\alpha\beta} + w_{,\tilde{\alpha}\tilde{\beta}}$. Scaling back $\varepsilon w \mapsto w$ and $x/\sqrt{\varepsilon}\mapsto x$, we have

$$\kappa_{\alpha\beta} = \kappa^0_{\alpha\beta} + w_{,\alpha\beta}. \tag{9}$$

Similarly, using (2) and (8), we find

$$F\cdot y_{,1} \approx F_p(\cos(\theta^0 - \theta_p) + \sqrt{\varepsilon}w_{,\bar{1}}\sin(\theta_p - \theta^0)). \tag{10}$$

Scaling back as before, we obtain

$$F\cdot y_{,1} \approx F_p(\cos(\theta^0 - \theta_p) + w_{,1}\sin(\theta_p - \theta^0)). \tag{11}$$

Finally, we turn to the peel front Γ. Recalling (2) and (8), and using the Taylor expansion,

$$y(x - \sqrt{\varepsilon}f\hat{e}_1) \approx y^0(x^0) - \sqrt{\varepsilon}fy^0_{,\alpha}(x^0)(\hat{e}_1)_\alpha + \varepsilon w(x^0/\sqrt{\varepsilon})n^0, \tag{12}$$

$$y_{,\alpha}(x - \sqrt{\varepsilon}f\hat{e}_1) \approx y^0_{,\alpha}(x^0) - \sqrt{\varepsilon}fy^0_{,\alpha\beta}(x^0)(\hat{e}_1)_\beta + \sqrt{\varepsilon}w_{,\tilde{\alpha}}(x^0/\sqrt{\varepsilon})n^0. \tag{13}$$

At both the perturbed and the straight peel front, the deformation and the slope are zero

$$y(x) = y_{,\alpha} = 0 \ \text{ on } \Gamma, \quad y^0(x) = y^0_{,\alpha} = 0 \ \text{ on } \Gamma^0. \tag{14}$$

Recalling that $y^0_{,11} = \kappa^0 n^0$, we conclude that in rescaled variables

$$w = 0, \quad w_{,1} = f\kappa^0, \quad w_{,2} = 0 \quad \text{on } \Gamma^0. \tag{15}$$

Finally, we require that

$$w \to 0 \tag{16}$$

as we go away from the peel front.

2.3. Governing equations

We apply the relations (9) and (11) to the potential energy (1) to obtain

$$\begin{aligned}\mathcal{E} = \int_{\Omega_r} \Big\{ &\frac{D}{2}((\kappa^0 + w_{,11})^2 + w_{,22}^2 + 2\nu(\kappa^0 + w_{,11})w_{,22} + (1-\nu)w_{,12}^2)\, dA \\ &- F_p(\cos(\theta^0 - \theta_p) + w_{,1}\sin(\theta_p - \theta^0))\Big\} dA - \int_{\Gamma_b} F{\cdot}y\, dl - \int_{\Omega_b} \gamma\, dA.\end{aligned} \tag{17}$$

We regard the singly curved surface with the tangential angle θ^0 and curvature κ^0 to be known and seek equations for the deformation w and the peel front. Therefore, we perturb them, $w \mapsto w + \eta v$, $f \mapsto f + \eta g$ and compute the first variation. Setting

$$\mathcal{E} = \int_{\Omega_r} \mathcal{F}(\nabla^2 w, \nabla w)\, dA - \int_{\Gamma_b} F{\cdot}y\, dl - \int_{\Omega_b} \gamma\, dA \tag{18}$$

where $\nabla^2 w$ denotes the second gradient (not Laplacian), it is a standard calculation to show

$$\begin{aligned}\delta\mathcal{E} = &\int_{\Omega_r} \left(\left(\frac{\partial \mathcal{F}}{\partial \kappa_{\alpha\beta}} \right)_{,\alpha\beta} - \left(\frac{\partial \mathcal{F}}{\partial t_\alpha} \right)_{,\alpha} \right) v\, dA \\ &+ \int_{\partial\Omega_r} \left(\frac{\partial \mathcal{F}}{\partial \kappa_{\alpha\beta}} v_{,\alpha} m_\beta - \left(\left(\frac{\partial \mathcal{F}}{\partial \kappa_{\alpha\beta}} \right)_{,\beta} - \frac{\partial \mathcal{F}}{\partial t_\alpha} \right) v m_\alpha \right) dl + \int_\Gamma \left(\mathcal{F} + \gamma \right) g\, dl\end{aligned} \tag{19}$$

where m is the unit outer normal to Ω_r. In this expression, the integral on the peeling front Γ results from the variations of the domain integral Ω_r. Since $\delta\mathcal{E} = 0$ for all $v \neq 0$ on Ω_r, it follows that

$$\left(\frac{\partial \mathcal{F}}{\partial \kappa_{\alpha\beta}} \right)_{,\alpha\beta} - \left(\frac{\partial \mathcal{F}}{\partial t_\alpha} \right)_{,\alpha} = 0. \tag{20}$$

Now,

$$\frac{\partial \mathcal{F}}{\partial \kappa_{\alpha\beta}} = \begin{pmatrix} D(\kappa^0 + w_{,11}) + 2\nu D w_{,22} & D(1-\nu)w_{,12} \\ D(1-\nu)w_{,12} & D w_{,22} + 2\nu D(\kappa^0 + w_{,11}) \end{pmatrix}, \tag{21}$$

$$\frac{\partial \mathcal{F}}{\partial t_\alpha} = \begin{pmatrix} F_p \sin(\theta_p - \theta^0) \\ 0 \end{pmatrix}, \tag{22}$$

and it follows that

$$\left(\frac{\partial \mathcal{F}}{\partial \kappa_{\alpha\beta}} \right)_{\alpha\beta} = D(\kappa^0_{,11} + \Delta^2 w), \tag{23}$$

$$\left(\frac{\partial \mathcal{F}}{\partial t_\alpha} \right)_{,\alpha} = - F_p \cos(\theta_p - \theta^0)\theta^0_{,1}. \tag{24}$$

We also recall the governing equation of the singly bent membrane (Xia et al., 2013) is

$$D\theta^0_{,11} - F_p \sin(\theta^0 - \theta_p) = 0 \tag{25}$$

or

$$D\theta^0_{,111} - F_p \cos(\theta_p - \theta^0)\theta^0_{,1} = 0. \tag{26}$$

Substituting (23), (24) and (26) in (20), and recognizing that $\kappa^0 = \theta^0_{,1}$, we find that the governing equation for the deformation of the film reduces to the usual small deflection bending equation:

$$\Delta^2 w = 0. \tag{27}$$

Turning to the boundary conditions, we note that on the peel front

$$v = 0, \quad v_{,1} = (\kappa^0 + w_{,11})g, \quad v_{,2} = 0 \tag{28}$$

analogous to (15). At the far surface, we expect w to decay and so $v \to 0$, $v_{,\alpha} \to 0$ as $x_2 \to \infty$. Therefore,

$$\delta\mathcal{E} = \int_{\mathcal{L}} \left(\frac{\partial \mathcal{F}}{\partial \kappa_{\alpha\beta}} v_{,\alpha} m_\beta - \left(\left(\frac{\partial \mathcal{F}}{\partial \kappa_{\alpha\beta}} \right)_{,\beta} - \frac{\partial \mathcal{F}}{\partial t_\alpha} \right) v m_\alpha \right) dl + \int_{\Gamma} \left(-\frac{\partial \mathcal{F}}{\partial \kappa_{11}} (\kappa^0 + w_{,11}) + \mathcal{F} \right) g \, dl \tag{29}$$

where $\mathcal{L}$ are the lateral surfaces. We obtain natural boundary conditions on $\mathcal{L}$ and identify the driving force on the peel front Γ to be

$$G = \frac{\partial \mathcal{F}}{\partial \kappa_{11}} (\kappa^0 + w_{,11}) - \mathcal{F} - \gamma \tag{30}$$

Recalling the definition of $\mathcal{F}$ and (23), noting that $w=0$ on Γ implies that all x_2 derivatives vanish, recalling from Xia et al. (2013) that

$$\frac{D}{2}(\kappa^0)^2 = \frac{F_p}{1 - \cos\theta_p} := G_\infty, \tag{31}$$

and linearizing in w, we conclude that the driving force on the peel front Γ is given by

$$G = G_\infty + D\kappa^0 w_{,11} - \gamma. \tag{32}$$

Finally, we invoke a rate-dependent heterogeneous evolution law for the peel front Γ in the form of a kinetic relation

$$\begin{cases} G + \gamma \le G_c(0, x_1, x_2) & \text{if } \dot{f} = 0, \\ G + \gamma = G_c(\dot{f}, x_1, x_2) & \text{if } \dot{f} > 0 \end{cases} \tag{33}$$

where G_c is the rate-dependent critical energy release rate (due to both surface energy and dissipative effects). Combining with (32), we obtain

$$\begin{cases} G_\infty + D\kappa^0 w_{,11} \le G_c(0, x_1, x_2) & \text{if } \dot{f} = 0, \\ G_\infty + D\kappa^0 w_{,11} = G_c(\dot{f}, x_1, x_2) & \text{if } \dot{f} > 0. \end{cases} \tag{34}$$

In summary, the perturbation w on the film deformation is given by the (27) subject to (15) and natural boundary conditions on $\mathcal{L}$ while the evolution of the front is given by (34). Note that this is a coupled problem.

2.4. Governing equations for the peel front

We now seek to solve for w and write down an explicit equation for the evolution of the front. We solve (27) by separation of variables:

$$w = \frac{1}{2\pi} \int_{-\infty}^{\infty} W_k(x_1) \exp(ikx_2) \, dk \tag{35}$$

So, (27) reduces to

$$W_k'''' - 2k^2 W_k'' + k^4 W_k = 0 \tag{36}$$

where the prime denotes differentiation with respect to x_1. The solution to (36) subject to the boundary conditions (15) and

(16) is

$$W_k(x_1) = \kappa^0 x_1 \ \exp(-|k|x_1)\hat{f}(k) \tag{37}$$

where $\hat{f}(k)$ is the Fourier transform of the peel front increment f. It follows from (32) that the Fourier transform of the energy release rate is given by

$$\hat{G}(k) = 2\pi G_\infty \delta(k) + 2D(\kappa^0)^2|k|\hat{f} = G_\infty(2\pi\delta(k) - 4|k|\hat{f}). \tag{38}$$

Taking the inverse Fourier transform of (38), we find

$$G(x_2) = G_\infty - \frac{4G_\infty}{\pi} PV \int_{-\infty}^{\infty} \frac{f(\xi) - f(x_2)}{(\xi - x_2)^2}\, d\xi \tag{39}$$

where PV denotes the Hadamard principal value of the integral. We substitute this in (34) to obtain an evolution equation for f that is in general a nonlinear, nonlocal equation.

2.5. Comments

We make a series of comments before we proceed. First, the energy release rate (39) is non-local in the sense that it depends on the entire shape of the peel front. The second term, the integral, may be regarded as the stiffness of the peel front. Physically, this stiffness reflects the fact that a wavy interface leads to a corrugated film and in turn an increase in the bending energy of the film.

Second, this result agrees with that of Legrand et al. (2011) who consider a crack lying on the mid-plane of a plate in the context of a *small* deformation plate theory. Further, it also agrees up to a factor with that of Rice (1985) who considered a perturbed crack front in an infinite medium, that of Hirth and Lothe (1992) who consider a perturbed dislocation and that of Dondl and Bhattacharya (2015) who consider a perturbed phase boundary. Thus peeling of heterogeneous adhesive films serves as a good model system to study various phenomena.

Third, if the critical energy release rate is linear in the velocity: i.e., if $G_c = G_c^0(x_1, x_2) + \mu\dot{f}$, then the evolution law can be written in Fourier variables as

$$G_\infty(2\pi\delta(k)) - 4|k|\hat{f}) = G_c^0(\widehat{f(x_2), x_2)}) + \mu\dot{\hat{f}} \tag{40}$$

Dondl and Bhattacharya (2015) have shown that if G_c^0 is periodic, then there is a critical effective adhesive strength $\bar{G}_c$ such that the interface is pinned whenever $G_\infty \le \bar{G}_c$. This effective adhesive strength depends on the microstructure and may both be anisotropic and asymmetric.

2.6. Steady propagation for an invariant pattern

When the adhesive heterogeneity is only a function of x_2 (i.e., it is uniform in the direction of propagation of the film) and the peeling force is held constant, then the peel front propagates in a steady manner after an initial transient. In other words,

$$f(x_2, t) = f_0(x_2) + Vt \tag{41}$$

where we take the average of f_0 to be zero. It follows $\dot{f} = V$ constant and $G_c = G_c(V, x_2)$. We can now combine (34) and (38) to obtain

$$\hat{f}_0 = \frac{1}{4|k|}\left(2\pi\delta(k) - \frac{\hat{G}_c}{G_\infty}\right). \tag{42}$$

We can evaluate this at $k=0$, recall that $\hat{f}_0(0) = 0$ since f_0 has zero average and conclude that

$$G_\infty = \bar{G}_c. \tag{43}$$

In other words, the overall adhesive strength is equal to the average of the point-wise adhesive strength in this special case.

2.7. Displacement control

We derived the governing equations above assuming the applied F to be a dead load. Unfortunately, this is difficult to pursue in experiment. So the experiments described below are displacement controlled where we prescribe the velocity at the far end of the film and measure the load. The governing equations described above still hold; however, we need a strategy to solve for F_p as a function of time. We do so by using the mechanics of the singly bent surface and specifically (25) to derive a relationship between the rate of change of applied force F_p, velocity of the point of application of force v_p and the

velocity of the peel front v_p. We assume that the displacement is applied in such a manner that the limiting angle far away is held fixed.

We define

$$u_p = (y(x_1^\infty) - y(x_1^0))\cdot\{\cos\theta^0, 0, \sin\theta^0\} - (x_1^\infty - x_1^0) = \int_{x_1^0}^{x_1^\infty} (\cos(\theta^0 - \theta^p) - 1)\, dl \tag{44}$$

where x_1^0 is the position of the peel front and x_1^∞ is the position of the application of the load. We can directly integrate Eq. (25) – multiply by $\theta_{,1}^0$ to integrate once, solve for $\theta_{,1}^0$ and integrate again – and obtain

$$u_p = \sqrt{\frac{4D}{F_p}}\left(\cos\left(\frac{\theta_p}{2}\right) - 1\right) \tag{45}$$

in the limit when $x_1^\infty \to 0$. Differentiating with respect to time, we find,

$$\dot{u}_p = \sqrt{D}\left(1 - \cos\left(\frac{\theta_p}{2}\right)\right)F_p^{-3/2}\dot{F}_p \tag{46}$$

Similarly, differentiating (45) with respect to time and noting that $v_p = \overline{\dot{y}(x_1^\infty)}\cdot\{\cos\theta^0, 0, \sin\theta^0\}$ and $v_f = -\overline{\dot{x}_1^0}$, we find

$$\dot{u}_p = v_p - v_f(1 - \cos\theta_p) \tag{47}$$

Equating the two and set v_f to be the average over the peel front of the incremental peel-front velocity, we find

$$v_p - \dot{f}_{\text{ave}}(1 - \cos\theta_p) = \sqrt{D}\left(1 - \cos\left(\frac{\theta_p}{2}\right)\right)F_p^{-3/2}\dot{F}_p. \tag{48}$$

We are now in a position to solve the problem under displacement controlled conditions. We employ an explicit forward-marching integration scheme as follows. Given v_p,

0. Initialize: Start with a straight peel front $f^i = 0$ in a homogeneous region at $t^i = 0$;
1. Calculate the Fourier transform of the energy release rate $\hat{G}^i(k)$ at t^i according to (38) and take the inverse Fourier transform of $\hat{G}^i(k)$ to obtain G^i;
2. Compute the peel-front velocity $\dot{f}^i$ according to the rate-dependent evolution law (34);
3. Compute the rate of change in peel force using (48);
4. Move forward by Δt and compute new f and F_p at $t^{i+1} = t^i + \Delta t$ using the Euler forward method:

$$f^{i+1} = f^{i+1} + \dot{f}^i\Delta t \tag{49}$$

$$F_p^{i+1} = F_p^{i+1} + \dot{F}_p{}^i\Delta t \tag{50}$$

5. Calculate $G_\infty^{i+1} = F_p^{i+1}(1 - \cos\theta_p)$;
6. Go to step 1 and continue the numerical integration until the peeling process is complete.

The step size used for the explicit integration is adjusted automatically so that the peel-front advance at each step is less than 0.02% of the minimum feature size of the heterogeneous pattern. Additional numerical simulations are also performed with finer step sizes and do not show noticeable change in the simulated peel-front evolution as well as the peel-force response, thereby confirming the numerical stability and convergence of the integration scheme.

3. Experiment

3.1. Specimen preparation

Peel test experiments were carried out using a model thin film system with well-controlled adhesive heterogeneity. The material system comprised of a polydimethylsiloxane (PDMS) sheet attached to a transparency film with an ink pattern. The adhesion energies of PDMS on ink and bare transparency surface have a large difference, allowing for heterogeneous patterning of interfacial adhesion with a spatial resolution of about 0.04 mm. Each heterogeneous test specimen was prepared according to following procedure. A desired heterogeneous pattern was generated using MATLAB and printed onto a transparency film with a commercial laser printer. The unpatterned side of the transparency film was then glued to a glass plate and held flat with a strong spray-on adhesive. A PDMS sheet was prepared by mixing the elastomer and curing agent of PDMS (Sylgard 184, Dow Corning Co.) at a weight ratio of 10:1 and degassing in a vacuum chamber for 30 min to remove

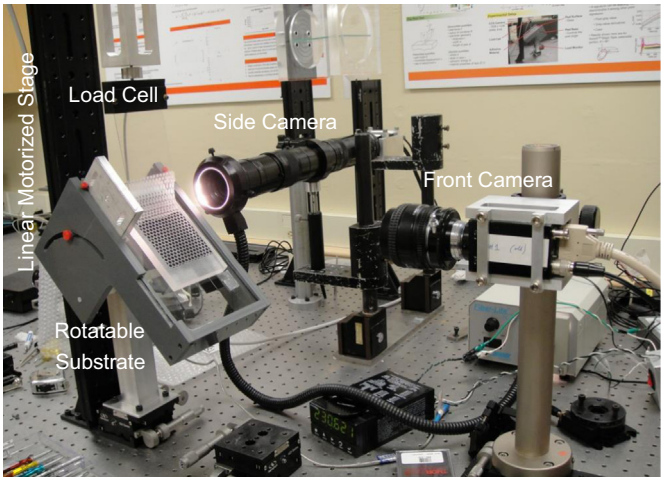

Fig. 2. Photograph of a peel test setup used for studying the effective adhesion and peel-front dynamics of a heterogeneous thin film.

trapped air bubbles. The liquid PDMS premix was subsequently casted over the rigidly supported transparency film, followed by curing at room temperature for 24 h and then 80 °C for 1 h. This two-stage curing treatment was necessary to minimize the residual stress in cured PDMS.

3.2. Peel testing

The effective adhesion between the PDMS sheet and patterned transparency was measured using a peel test setup as shown in Fig. 2. The flat substrate was mounted on a rotatable table which was used for precisely controlling the peel angle.

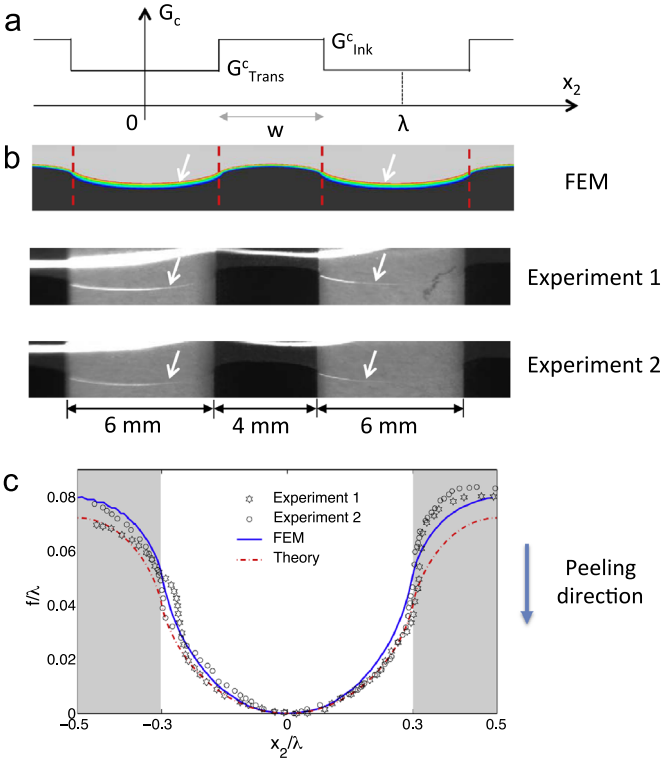

Fig. 3. Peel front perturbation of a stripe-patterned interface. (a) Variations of the intrinsic adhesion energy along the front direction x_2. The ink strips of width $w=4$ mm are aligned along the peeling direction, and have a higher adhesion energy G^c_{Ink} than the rest of the interface of adhesion energy G^c_{Trans}. (b) Snapshots of propagating peel fronts obtained from a finite element simulation and two independent experiments. The peel front positions are marked with white arrows. (c) Comparison of the theoretical peel-front geometry to the simulation and experimental results. (For interpretation of the references to color in this figure caption, the reader is referred to the web version of this paper.)

The PDMS sheet was peeled off from the substrate at a constant peel speed using a vertically mounted linear stage. The corresponding peel force was recorded by a load cell with 200 g load capacity. The transparent nature of PDMS allowed direct observation of the peel front during peeling. Two digital CCD cameras equipped with high-magnification lenses were positioned in front and to the side of the PDMS sheet and used to record in situ the evolution of the peel-front profile. Peel tests were also performed on homogeneous specimens with uniform adhesive strength to obtain the intrinsic adhesion energies of the PDMS–ink and PDMS–transparency interfaces. The intrinsic adhesion energies were measured to be $3.53v^{0.25}$ J/m^2 for the PDMS–ink interface and $0.65v^{0.25}$ J/m^2 for the PDMS–transparency interface. Here v is the peel-front velocity in the unit of μm/s.

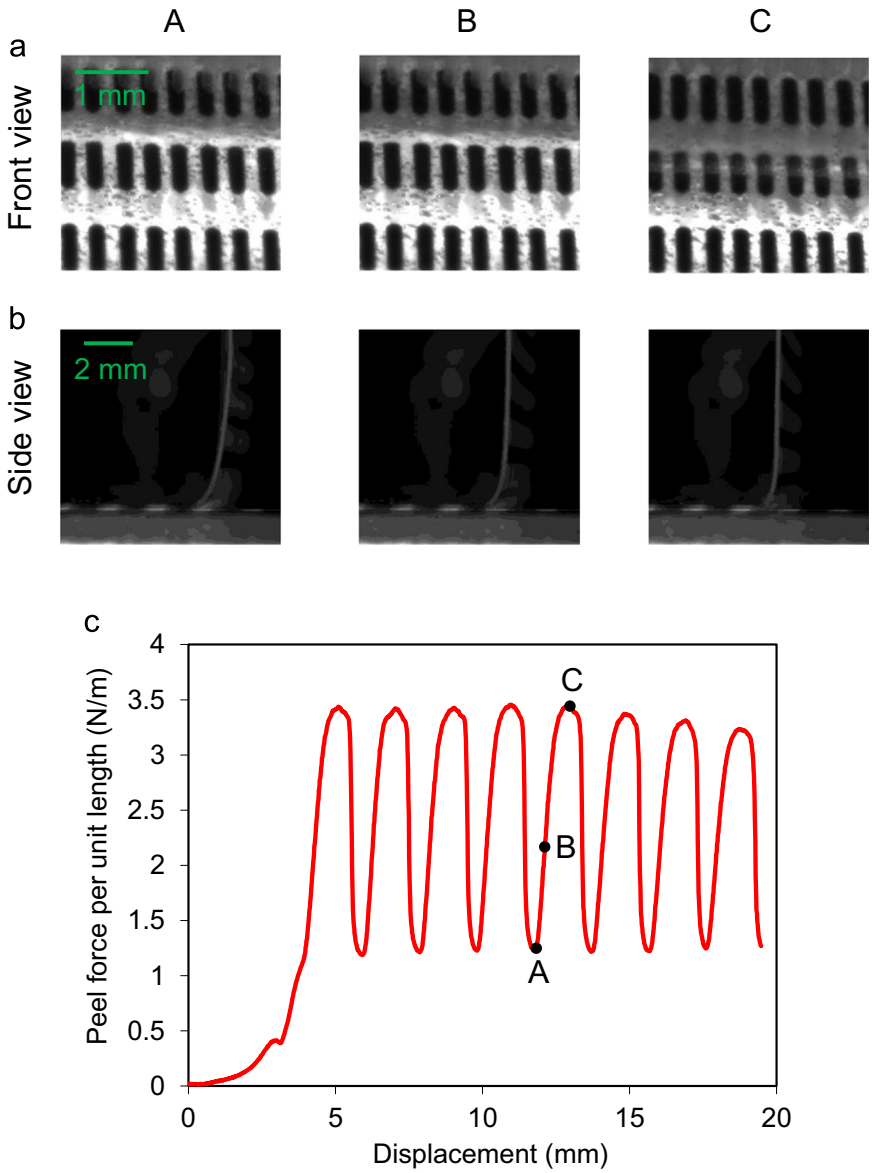

Fig. 4. Results for a PDMS film peeled from a patterned (strips-of-stripes) substrate. (a) Top view showing the position of the peel front with respect to the striped pattern on the substrate. (b) Side view showing the evolution of the radius of curvature of the film. (c) Peel force per unit length as a function of applied displacement. The snapshots correspond to the marked instants (A–C) on the peel force curve in (c). The peel angle is 90°.

4. Results and discussion

4.1. Stripes

We begin with a simple one-dimensional (1-D) heterogeneous pattern made of a row of uniformly spaced ink stripes with period $\lambda=10$ mm that are oriented along the peeling direction x_1. Fig. 3(a) shows the distribution of adhesion energy as a function of x_2. The stripes of width $w=4$ mm are characterized by the adhesion energy G^c_{Ink} while the rest of the interface is characterized by the adhesion energy G^c_{Trans}. The bottom two images in Fig. 3(b) show the steady-state profiles of the peel front obtained in two separate experiments. As the PDMS film (width $b=50$ mm and thickness $t=1.2$ mm) is peeled, the peeling front becomes wavy as it tries to go ahead in the weaker transparency region but is held back in the tougher ink region. The two experimental peel-front profiles are extracted through image processing and plotted along with the theoretical prediction in Fig. 3(c).

Fig. 3(c) also shows the theoretical curve obtained from (42). In this case, we can expand G_c and f_0 in a Fourier series to obtain

$$\delta f(x_2) = f(0) - f(x_2) = -f_0(x_2) = C\frac{\lambda}{4\pi^2}\sum_{m=1}^{+\infty}\frac{\sin(m\pi w/\lambda)}{(-1)^{m+1}m^2}\cos(2\pi m z/\lambda) \tag{51}$$

The contrast is defined as $C=(G^c_{\text{Ink}}-G^c_{\text{Trans}})/G^c_{\text{eff}}$ where G^c_{eff} is the average adhesion energy of the interface (see Vasoya et al., 2013 for the analogous result in fracture). We observe good agreement between the experiments and the theoretical model.

A finite element analysis was also carried out to further verify the model. The peeling process was simulated using a cohesive zone model (CZM) in which a bilinear cohesive zone law (Camacho and Ortiz, 1996) was employed. The simulated cohesive zone geometry is shown in the top image of Fig. 3(b) as a colored band. The color contour in the image indicates

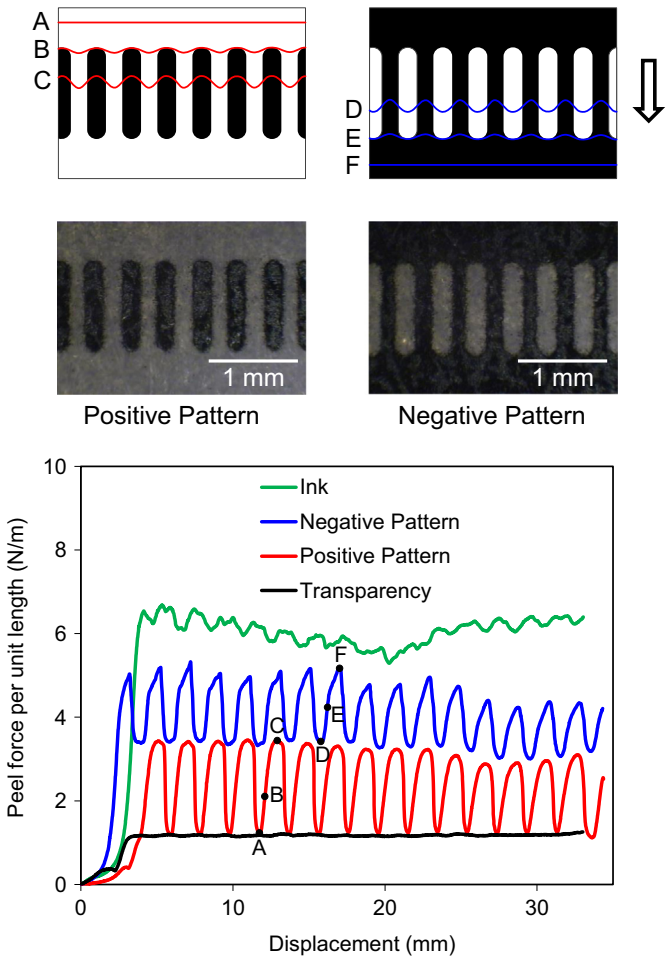

Fig. 5. Peel force per unit length vs. applied displacement for PDMS films peeled from positive and negative strips-of-stripe patterns as well schematic illustration of the peel front positions. Also shown are the results for peeling of two PDMS films from a bare transparency and a fully inked substrate. The peel angle is 90°.

the opening displacement within the cohesive zone. The middle line of the cohesive zone is shown in Fig. 3(b), and a good agreement with the theoretical result is again observed.

4.2. Strips of stripes

We turn to a more complex microstructure as shown in Fig. 4. A PDMS film (width $b=50$ mm and thickness $t=0.2$ mm) was peeled from a substrate with a strips-of-stripes pattern. The pattern seen in Fig. 4(a) consists of periodically distributed ink stripes of finite length (1 mm) and width (0.2 mm). The period of the stripes is $\lambda=0.4$ mm. The far-field peel angle was kept constant at 90°. The curvature of the film (side view) and the advancing peel front on the substrate (top view) were continuously recorded using the two CCD cameras. The measured peel force/unit length vs. applied displacement is shown in Fig. 4(c). The peel force exhibits an oscillatory behavior with a constant period. The snapshots of the top view and front view at three different instants marked as A–C on the peel force curve are shown in Fig. 4(a) and (b), respectively.

At the instant A when the peel force is in a valley, we see from the snapshots that the peel front is almost straight and in the middle of the region with no ink (recall that the bare transparency has lower adhesion). We also see from the side view that the curvature of the film at the front is low compared to the other two instances. The peel force is close to that of a homogeneous system with bare transparency (more on this comparison later). As the peel front reaches the printed stripes of higher adhesion, the peel front becomes wavy, the curvature of the film viewed from the side increases and the peel force increases as in the instant B. The peel force reaches its peak at the instant C. We note from the side view that the curvature of the film at the peel front is extremely high, and from the top view that the front has penetrated the printed region. In a perfectly rate-independent setting, we would expect the peak to occur as the front is pinned at the bare transparency – printed stripes interface. The fact that the peak occurs slightly beyond this is a manifestation of rate effects. After the instant C, the peel process becomes unstable and shows a snap-through behavior. Correspondingly, the peel force drops quickly as the peel front passes through the inked region, exits the inked region and becomes straight. Each period in the peel force vs. displacement curve corresponds to the front traversing through one row of stripes.

The peel force vs. displacement curve for peeling a PDMS film from a substrate with the pattern above (positive pattern) is contrasted with that from a substrate with a negative pattern (i.e., stripes of bare transparency surrounded by ink) in Fig. 5. Recall that the adhesive energy is higher for the inked region in comparison to the bare transparency. Therefore the peel force oscillates at a higher level for the negative pattern. The valleys of the peel force for the negative pattern

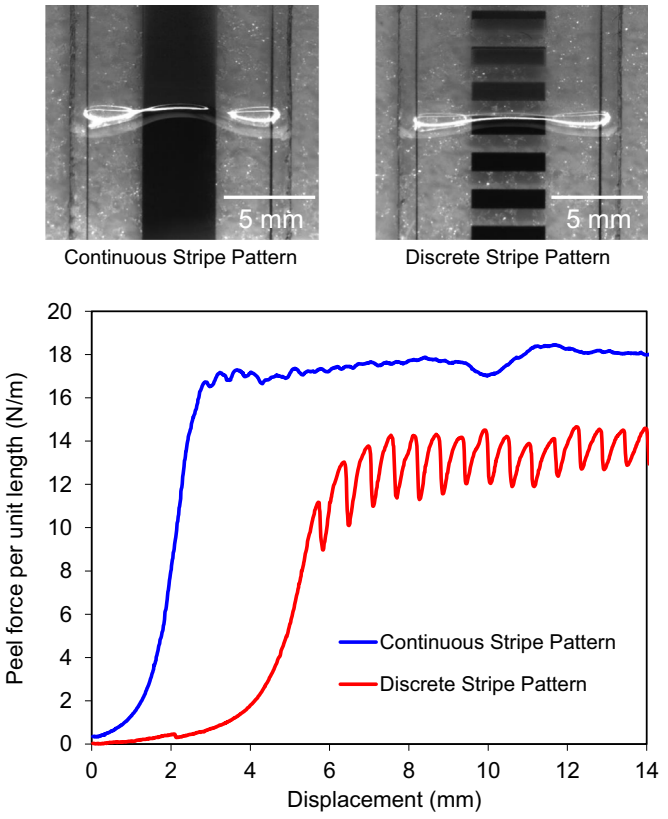

Fig. 6. Peel force per unit length vs. applied displacement for PDMS films peeled from a continuously striped pattern and a discretely striped pattern. The peel front advances in the downward direction in both cases. The peel angle is 45°.

correspond to the instant D when the peel front is propagating through the striped region, while the peaks correspond to the instant F when the peel front just penetrates into the fully inked region. Similar to the positive pattern case, a snap through instability is observed after the peel force reaches its peak at the instant F. Once again, the peak occurs beyond the interface as a manifestation of rate effects.

Note that the valleys of the peel force for the positive pattern match the force for peeling from a homogeneous bare transparency. Furthermore, the peaks of the positive pattern correspond to the valleys of the negative pattern. This indicates that the critically pinned peel-front shape at the instant C in the former case is identical to the peel-front configuration at the instant D in the latter case. However, the peaks of the force for the negative pattern do not match the force for peeling from a homogeneous fully inked substrate. This reflects the fact that the resistance of the peel front is nonlocal and depends on the entire shape (rather than the local value) and the fact that the intrinsic adhesion strength of our material system has a rate dependence. This phenomenon requires further investigation.

The results for peel force vs. displacement for a broken stripe pattern together with a continuous stripe pattern (similar to Fig. 3(a)) are shown in Fig. 6. The width of the stripes in both cases is the same, $w=4$ mm, and the center-to-center spacing between the discrete stripes of the inked region is 2 mm while the thickness of the stripes is 1 mm. The width of the PDMS film is $b=10$ mm and its thickness is $t=1.2$ mm. The peel angle at the far end is fixed at 45°. It is noted that in the case of peeling from the continuous stripe, following an initial transient, a steady-state perturbed peel front propagates along the strip direction and the corresponding peel force is constant. In the case of the discrete stripes, the peel force oscillates with a regular period as the peeling progresses. The peaks of the peel force correspond to the instant at which the peel front is in the middle of the discrete ink stripes. The valleys of the peel force correspond to the instant when the peel front is at a

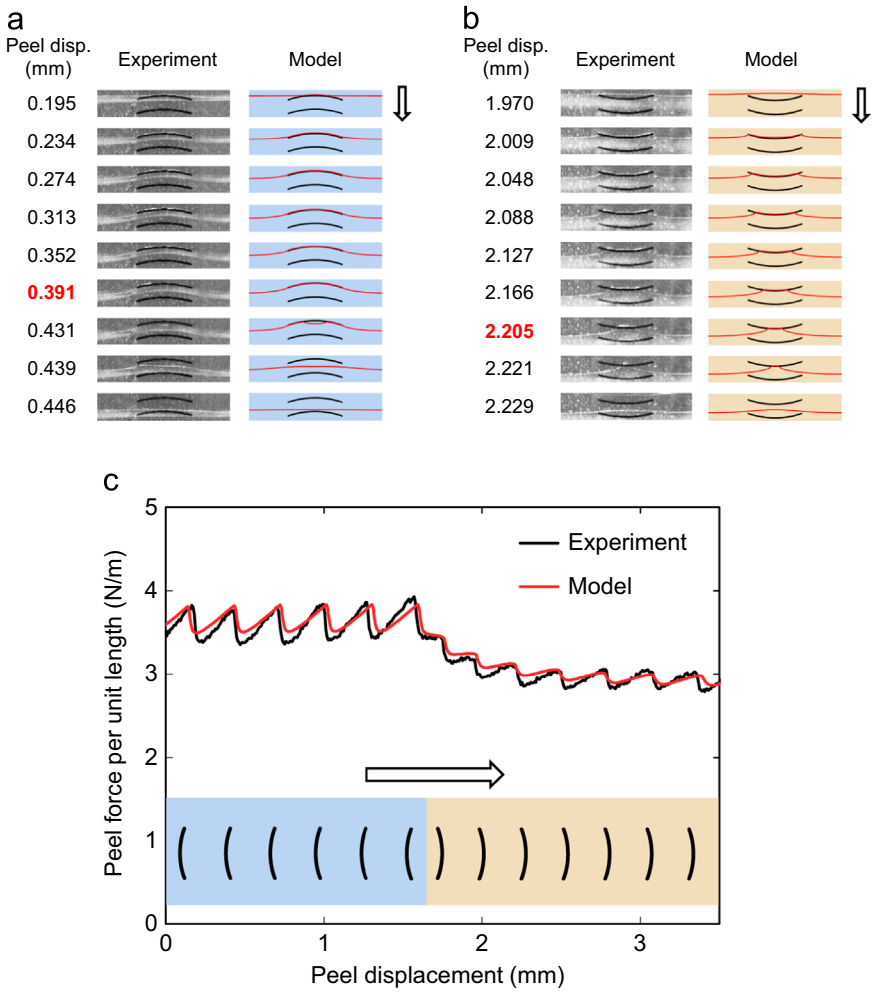

Fig. 7. Adhesive directionality shown by a heterogeneous interface with arc patterns. (a) Peel-front evolution in the hard peeling direction predicted by the model (right) and compared with the experimental measurement (left). (b) Peel-front evolution of the same film peeled in the opposite direction. (c) Comparison between the computational and experimental peel-force curves. In (a) and (b), the peel displacement at which the peel force reaches a local peak (i.e., at critical pinning stage) is marked in bold red. (For interpretation of the references to color in this figure caption, the reader is referred to the web version of this paper.)

location in the middle of the bare transparency region. The period of the oscillating force corresponds to the distance between the centers of neighboring ink stripes. The mechanistic explanation for the oscillatory force and the corresponding value of the peak (valley) force is similar to the ones provided earlier. It is worth noting that the peak force for the discrete pattern does not match the steady-state force for peeling from the continuous stripe pattern. This may be due to the small thickness of the discrete stripe pattern, which does not allow the perturbed peel front to fully develop into the steady-state configuration of the continuous stripe pattern as shown in Fig. 6(a).

4.3. Asymmetric pattern

We further demonstrate, through both modeling and experimentation, that remarkable adhesion directionality can be achieved with an asymmetric 2-D pattern. Fig. 7 shows the geometry of the pattern, which has a circular arc shape of constant thickness. A periodic heterogeneous microstructure was created by replicating the pattern along the vertical direction at a spatial period of 1.0 mm. The geometric parameters of the pattern were: PDMS sheet width $b=10.0$ mm, thickness $t=1.2$ mm, arc width $w=4.0$ mm, arc radius $R=6.1$ mm, and arc thickness $h=0.1$ mm. The test specimen included two microstructured regions with the arc pattern pointing in opposite directions as shown in the inset of Fig. 7(c). This design allowed a quick examination of the effective adhesive strength in both directions using a single test and removed artifacts due to variations in sample preparation and the like.

As shown in the Fig. 7(c), the peel force predicted by the model oscillates as it passes each column of the arc-shaped areas of higher adhesion strength. A 25% higher effective adhesive strength is observed in the hard peeling direction for which the convex portion of the arc touches the peel front first, compared to that in the opposite easy direction. The experimentally measured peel force shows the same expected peeling behavior. The physical origin of the observed directionality is obvious from a close inspection of the peel-front evolution. Fig. 7(a) and (b) shows the experimental and computational peel-front snapshots in the hard and easy peeling directions as the peeling process progresses. When the front propagates in the hard direction, it first encounters the convex side of the arc and gets pinned against a large portion of the arc, as seen in Fig. 7(a). Consequently, the arc is seen as a significant obstacle which requires a large peel force to overcome. After the peel force reaches the maximum value, depinning of the front first occurs near the center of the arc and spreads quickly towards the ends of the arc, resulting in a drop in the peel force. In contrary, the non-local negotiation of the peel front with the same arc in the opposite direction leads to a different front pinning and depinning behavior, as seen in Fig. 7(b). As the peel front encounters the arc in this direction, it first touches and bypasses the two arms of the arc in a progressive manner. The critical pinning site in this case is located in the narrow central portion of the arc. Therefore, the peel front sees the arc as a smaller obstacle which requires a smaller peel force to overcome.

5. Conclusions

We have presented results for the manipulation of effective adhesion strength through patterning of interfacial surfaces. The effects of adhesive heterogeneity have been demonstrated for patterns of various shapes and sizes including periodic one- and two-dimensional patterns. It has been demonstrated both theoretically and experimentally that the effective adhesion is a collective response of the peel front perturbation to the overall pattern. A theoretical model based on the Kirchhoff plate theory via a variational formulation has been developed to predict the peel-front distortion due to adhesive heterogeneity, which agrees well with the experimental measurement performed on a model material system. By choosing an appropriate pattern, it is possible to create anisotropy as well as asymmetry in effective adhesion strength. In the present study, an arc-shaped pattern has been used to illustrate remarkable adhesion directionality. It is shown that varying adhesion strengths can be attained depending on the direction of peeling with respect to the shape of the pattern. The adhesion strength is higher when the peel front propagates towards the convex side of the arc pattern in comparison to when the peel front propagates towards the concave side of the pattern. However, to achieve macroscopic effects through adhesive heterogeneities, certain conditions must be fulfilled. First, the dissipative failure mechanisms taking place at the peel front vicinity must be confined in a zone much smaller than the feature size of the heterogeneous pattern introduced at the interface. In the other limit investigated in Chen et al. (2008), when the cohesive zone is larger than the heterogeneity size, the details of the adhesion energy landscape are smoothed out and the macroscopic peeling response of the film depends essentially on the average adhesion energy. Furthermore, the heterogeneities must be introduced at a scale sufficiently small with respect to the characteristic bending radius of the film to create non-local interactions between the peel front and heterogeneities. In other words, patterning the adhesion energy offers new venues for designing adhesives with new and better properties, but this pattern must be introduced at the proper length scale.

While the effective adhesion strength for a selected set of heterogeneous patterns has been investigated in the present study, a number of questions remain unanswered. Since the patterning considered here is two dimensional, there are infinite choices for the shape, size and spacing of the patterns. A new optimization approach is required to identify optimal patterns that will result in desired adhesion properties. The patterns that have been explored in this study have been mostly oriented perpendicular to the peeling direction. For general applications, it may be necessary to explore the effect of the directionality and orientation of the patterns with respect to the peeling direction. This will provide additional insights into the mechanics of front propagation and adhesive heterogeneity. The present study has focused exclusively on periodic

patterns and their effects on effective adhesion strength. It would be interesting to explore the effects of random or non-periodic patterning and multi-shape patterning on peeling and potential optimization of patterns for desired properties such as enhancement, anisotropy and asymmetry. The analytical model based on the Kirchhoff plate theory presented in this paper is general enough to include both bending and twisting of the film but is limited to the treatment of problems with negligible in-plane extensibility. At low angles of peeling, the effects of in-plane extensibility, friction and slip at the adhesive interface could be important (Begley et al., 2013) and need to be accounted for in the model.

The peeling of heterogeneous thin films from a heterogeneous substrate serves as an excellent model system for studying heterogeneous materials. It could be of value in furthering our understanding of various phenomena in heterogeneous materials including, brittle fracture (Rice, 1985; Legrand et al., 2011), dislocations (Hirth and Lothe, 1992), phase boundaries (Dondl and Bhattacharya, 2010) and wetting fronts (Joanny and de Gennes, 1984). A recent theoretical and computational study has suggested mechanisms and architecture for toughening of composite materials (Hossain et al., 2014). The findings from the present study can be extended to the design of realistic heterogeneous materials such as composites and failure resistant materials with enhanced toughness. The recent advances in digital manufacturing techniques such as 3D printing are providing new ability to synthesize materials with complex and precise heterogeneities. Integrated with these new routes of material synthesis, the insights gained in this study could potentially provide new directions and paradigms for design and fabrication of new materials with extraordinary properties.

Acknowledgment

Much of this work was carried out while S.X. and L.P. held positions at the California Institute of Technology. We gratefully acknowledge the financial support of the US National Science Foundation (through DMR-0520565 (all authors) and CMMI-1201102 (G.R. and K.B.)), the 'PhyCrack' Marie Curie Outgoing Fellowship No. 220494 and the 'ToughBridge' Marie Curie Integration Grant No. 294025 from the European Union (L.P.).

References

Begley, M.R., Collinoa, R.R., Israelachvili, J.N., McMeeking, R.M., 2013. Peeling of a tape with large deformations and frictional sliding. J. Mech. Phys. Solids 61, 1265–1279.
Bower, A.F., Ortiz, M., 1991. A 3-dimensional analysis of crack trapping and bridging by tough particles. J. Mech. Phys. Solids 39 (6), 815–858.
Bower, A.F., Ortiz, M., 1993. The influence of grain-size on the toughness of monolithic ceramics. J. Eng. Mater.—Trans. ASME 115, 228–236.
Camacho, G., Ortiz, M., 1996. Computational modelling of impact damage in brittle materials. Int. J. Solids Struct. 33 (20), 2899–2938.
Chan, E.P., Ahn, D., Crosby, A.J., 2007. Adhesion of patterned reactive interfaces. J. Adhes. 83 (5), 473–489.
Chen, B., Shi, X., Gao, H., 2008. Apparent fracture/adhesion energy of interfaces with periodic cohesive interactions. Proc. R. Soc. A: Math. Phys. Eng. Sci. 464 (2091), 657–671.
Chung, J.Y., Chaudhury, M.K., 2005. Roles of discontinuities in bio-inspired adhesive pads. J. R. Soc. Interface 2 (2), 55–61.
Cox, B., Yang, Q.D., 2006. In quest of virtual tests for structural composites. Science 314 (5802), 1102–1107.
Craciun, B., Bhattacharya, K., 2004. Effective motion of a curvature-sensitive interface through a heterogeneous medium. Interfaces Free Bound. 6, 151–174.
Dalmas, D., Barthel, E., Vandembroucq, D., 2009. Crack front pinning by design in planar heterogeneous interfaces. J. Mech. Phys. Solids 57 (3), 446–457.
Démery, V., Rosso, A., Ponson, L., 2014. From microstructural features to effective toughness in disordered brittle solids. EPL (Europhys. Lett.) 105 (3), 34003.
Dirr, N., Yip, N., 2006. Pinning and de-pinning phenomena in front propagation in heterogeneous media. Interface Free Bound. 8 (1), 79–109.
Dondl, P., Bhattacharya, K., 2015. Effective behavior of an interface propagating through a periodic elastic medium. Interface Free Bound. To appear.
Dondl, P.W., Bhattacharya, K., 2010. A sharp interface model for the propagation of martensitic phase boundaries. Arch. Ration. Mech. Anal. 197, 599–617.
Ghatak, A., Mahadevan, L., Chung, J.Y., Chaudhury, M.K., Shenoy, V., 2004. Peeling from a biomimetically patterned thin elastic film. Proc. R. Soc. Lond. Ser. A: Math. Phys. Eng. Sci. 460 (2049), 2725–2735.
Greiner, C., del Campo, A., Arzt, E., 2007. Adhesion of bioinspired micropatterned surfaces: effects of pillar radius, aspect ratio, and preload. Langmuir 23 (7), 3495–3502.
Guo, P., Zheng, Y., Liu, C., Ju, J., Jiang, L., 2012. Directional shedding-off of water on natural/bio-mimetic taper-ratchet array surfaces. Soft Matter 8 (6), 1770–1775.
Hirth, J.P., Lothe, J., 1992. Theory of Dislocations. Krieger Publishing Company, Malabar.
Hossain, M., Hsueh, C.-J., Bourdin, B., Bhattacharya, K., 2014. Effective toughness of heterogeneous media. J. Mech. Phys. Solids 71, 15–32.
Hutchinson, J.W., Suo, Z., 1992. Mixed-mode cracking in layered materials. Adv. Appl. Mech. 29, 63–191.
Jin, F., Guo, X., 2013. Mechanics of axisymmetric adhesive contact of rough surfaces involving power-law graded materials. Int. J. Solids Struct. 50 (20), 3375–3386.
Joanny, J.F., de Gennes, P.G., 1984. A model for contact angle hysteresis. J. Chem. Phys. 81, 552–562.
Kesari, H., Doll, J.C., Pruitt, B.L., Cai, W., Lew, A.J., 2010. Role of surface roughness in hysteresis during adhesive elastic contact. Philos. Mag. Lett. 90 (12), 891–902.
Kesari, H., Lew, A.J., 2011. Effective macroscopic adhesive contact behavior induced by small surface roughness. J. Mech. Phys. Solids 59 (12), 2488–2510.
Kirchhoff, G., 1850. über das gleichgewicht und die bewegung einer elastischen scheibe. J. Reine Angew. Math. 40, 51–88.
Legrand, L., Patinet, S., Leblond, J.B., Frelat, J., Lazarus, V., Vandembroucq, D., 2011. Coplanar perturbation of a crack lying on the mid-plane of a plate. Int. J. Fract. 170, 67–82.
Milton, G.W., 2002. The Theory of Composites. Cambridge University Press, Cambridge.
Nemat-Nasser, S., Hori, M., 1999. Micromechanics: Overall Properties of Heterogeneous Materials. North-Holland Publishing Company, Amsterdam.
Patinet, S., Alzate, L., Barthel, E., Dalmas, D., Vandembroucq, D., Lazarus, V., 2013a. Finite size effects on crack front pinning at heterogeneous planar interfaces: experimental, finite elements and perturbation approaches. J. Mech. Phys. Solids 61 (2), 311–324.
Patinet, S., Bonamy, D., Proville, L., 2011. Atomic-scale avalanche along a dislocation in a random alloy. Phys. Rev. B 84 (17), 174101.
Patinet, S., Vandembroucq, D., Roux, S., 2013b. Quantitative prediction of effective toughness at random heterogeneous interfaces. Phys. Rev. Lett. 110 (16), 165507.
Ponson, L., Bonamy, D., 2010. Crack propagation in brittle heterogeneous solids: material disorder and crack dynamics. Int. J. Fract. 162 (1–2), 21–31.
Ponte Castañeda, P., Suquet, P., 1998. Nonlinear composites. Adv. Appl. Mech. 34 (998), 171–302.

Prakash, M., Bush, J.W., 2011. Interfacial propulsion by directional adhesion. Int. J. Non-Linear Mech. 46 (4), 607–615.
Ramrus, D.A., Berg, J.C., 2006. Enhancement of adhesion to heterogeneously patterned substrates. Colloid. Surf. A—Physicochem. Eng. Asp. 273 (1–3), 84–89.
Rice, J.R., 1985. 1st-order variation in elastic fields due to variation in location of a planar crack front. J. Appl. Mech.—Trans. ASME 52 (3), 571–579.
Rivlin, R.S., 1944. The effective work of adhesion. Paint Technol. 9, 215.
Santos, D., Spenko, M., Parness, A., Kim, S., Cutkosky, M., 2007. Directional adhesion for climbing: theoretical and practical considerations. J. Adhes. Sci. Technol. 21 (12–13), 1317–1341.
Vasoya, M., Leblond, J.-B., Ponson, L., 2013. A geometrically nonlinear analysis of coplanar crack propagation in some heterogeneous medium. Int. J. Solids Struct. 50 (2), 371–378.
Xia, S., Ponson, L., Ravichandran, G., Bhattacharya, K., 2012. Toughening and asymmetry in peeling of heterogeneous adhesives. Phys. Rev. Lett. 108 (May (19)), 196101.
Xia, S., Ponson, L., Ravichandran, G., Bhattacharya, K., 2013. Adhesion of heterogeneous thin films—I: elastic heterogeneity. J. Mech. Phys. Solids 61 (3), 838–851.
Xu, G., Bower, A.F., Ortiz, M., 1998. The influence of crack trapping on the toughness of fiber reinforced composites. J. Mech. Phys. Solids 46, 1815–1833.